Monte Carlo Uncertainty Quantification and Sensitivity Analysis for the C5G7 Benchmark

Kayla B. Clements [1,*], Todd S. Palmer[1], Aaron J. Olson[2], Gianluca Geraci[2], Ilham Variansyah[1]

[1]Oregon State University, Corvallis, Oregon; [2]Sandia National Laboratories, Albuquerque, New Mexico

[leave space for DOI, which will be inserted by ANS]

ABSTRACT

In this study, sampling methods and Monte Carlo (MC) radiation transport (RT) were used to perform uncertainty quantification (UQ) and global sensitivity analysis (GSA) on the 3D C5G7-TD benchmark in its initial unrodded configuration. UQ was performed using variance deconvolution, a recently-developed uncertainty propagation method for stochastic solvers that computes parametric variance by explicitly accounting for the stochastic solver's variance. Additionally, we applied our recent work integrating variance deconvolution with Sobol' sensitivity indices to compute Sobol' indices for eight input parameters – the density and radius of each of the four fuel types in the core. The C5G7 core was modeled using Monte Carlo Dynamic Code (MC/DC), an open-source neutral-particle transport code, and both the core k_{eff} eigenvalue and pinwise core fission rate distribution were considered as quantities of interest. Manufacturing uncertainties of fuel pin radius and density were sampled from a normal distribution of a 5% standard deviation about their respective nominal values. Variation of the densities and radii of the specific pin components such as pellet radius, gap thickness, and clad thickness was limited due to the spatial homogenization of the benchmark cross-sections. Using variance deconvolution allowed for more cost-efficient UQ and GSA with MC RT code than the standard approach of increasing particle count to reduce the solver variance.

Keywords: Monte Carlo transport, C5G7, uncertainty quantification, global sensitivity analysis

1. INTRODUCTION

It has remained consistently important for nuclear research, industry, safety, and regulation that best-estimate predictions from computational models and simulations be reported with their associated uncertainties. These requirements can be met using uncertainty quantification (UQ, also called uncertainty analysis) and sensitivity analysis, both of which are important steps in rigorous model validation. To propagate input uncertainties through reactor physics and modeling simulations, both deterministic [1] and statistical sampling methods [2, 3] have been widely proposed and applied for both nuclear data and manufacturing uncertainties. Deterministic approaches, such as approximating first-order sensitivity coefficients by perturbing parameters locally around their nominal values [1], typically require fewer model evaluations than sampling-based approaches and are therefore attractive for computational models for which even one evaluation is computationally expensive. However, these approaches make some assumptions about the linearity of the underlying function and allow for relatively small parameter perturbations. In sampling methods, uncertain parameters are sampled from their probability distributions and propagated through the model, then statistics of the quantity of interest are computed directly using sampling-based estimators [4]. Sampling-based methods are useful because they do not make assumptions about the linearity, smoothness, or regularity of the model

*clemekay@oregonstate.edu

response [4]; however, their primary drawback is the potential high computational cost associated with the multiple code evaluations needed to compute the required statistics with satisfactory precision [4], since an independent code evaluation is required for each drawn sample.

Sampling methods can become cost-prohibitive when the underlying solver itself is also stochastic, as is the case with Monte Carlo (MC) radiation transport (RT) solvers. When inputs to a stochastic simulator have some associated uncertainty, the total observed variance of the output is a combination of the variability of the solver itself ("solver variance") and the variability of the input parameters [3, 2]. To estimate variance and sensitivities of the output introduced solely by the uncertain input parameters ("parametric variance" and "parametric sensitivities"), a standard approach to handle the stochasticity of the solver is to increase the number of particle histories such that the solver variance is a relatively small contribution of the total observed variance; the high computational cost of doing so must be paid for each of the multiple code evaluations required for sampling methods.

As an alternative to the standard treatment we have proposed a variance deconvolution approach [5, 6], in which we compute parametric variance by explicitly quantifying and removing the solver variance from the total observed variance, rather than by minimizing the solver variance. In [5], we rigorously showed that variance deconvolution is accurate and much more cost-effective than the standard approach for computing parametric variance. In recent work [7], we integrated variance deconvolution into sampling estimators for sensitivity indices (SIs, also referred to as Sobol' indices), which is a GSA approach that uses analysis of variance to rank input parameters in order of importance to the output [4]. Exploration of the practical usability and benefit of these capabilities has included analytic functions and simple slab-geometry radiation transport problems with and without stochastic media. However, exploration on more realistic problems has not been performed, leaving questions as to the practical value for large-scale MC RT computations.

In this work, as an example of application to a more realistic MC RT problem, we use variance deconvolution to evaluate the parametric variance and perform sensitivity analysis on the 3D C5G7 criticality benchmark problem [8]. We propagate uncertainties of eight input parameters, namely, the radii and densities of the four fuel types in the core, to compute the k-eigenvalue and fission rate distributions across the core. We perform MC RT simulations with the Monte Carlo Dynamic Code (MC/DC), an open source neutron transport code developed by the PSAAP-III Center for Exascale Monte Carlo Neutron Transport [9].

The remainder of the paper is structured as follows. In Section 2, we summarize the variance deconvolution approach and its use for UQ and GSA. In Section 3, we briefly describe the C5G7 3D benchmark, then present and discuss the results. A summary and conclusions are provided in Section 4.

2. UNCERTAINTY AND GLOBAL SENSITIVITY ANALYSIS WITH VARIANCE DECONVOLUTION

In this section, we first summarize and introduce notation for UQ and GSA in a general context, then introduce the case of UQ and GSA for a stochastic solver. For a detailed presentation of variance deconvolution and an algorithmic representation of variance deconvolution for UQ, see [5].

2.1. Uncertainty and global sensitivity analysis

We consider a generic scalar quantity of interest (QoI) $Q = Q(\boldsymbol{\xi}), \boldsymbol{\xi} = (\xi_1, \ldots, \xi_k) \in \Xi \subset \mathbb{R}^k$, where $\xi_1, \ldots, \xi_k$ are independent random variables with arbitrary joint distribution function $p(\boldsymbol{\xi})$. To characterize

the effect of input uncertainty on Q, we are interested in statistics of Q, like its mean and variance,

$$\mathbb{E}_{\xi}\left[Q\right] = \int_{\Xi} Q\left(\boldsymbol{\xi}\right) p(\boldsymbol{\xi}) d\boldsymbol{\xi} \qquad \text{and} \qquad \mathbb{V}ar_{\xi}\left[Q\right] = \int_{\Xi} \Big(Q\left(\boldsymbol{\xi}\right) - \mathbb{E}_{\xi}\left[Q\right] \Big)^2 p(\boldsymbol{\xi}) d\boldsymbol{\xi}, \tag{1}$$

where a subscript indicates expectation and variance over ξ. We are also interested in computing SIs, which give the ratio of the conditional variance of a parameter or set of parameters to the unconditional parametric variance and are commonly used to rank the parameters in order of importance to the QoI [4]. The importance of parameter ξ_i can be described by its first-order SI $\mathbb{S}_i$ and its total-order SI $\mathbb{T}_i$,

$$\mathbb{S}_i = \frac{\mathbb{V}ar_{\xi_i}\Big[\mathbb{E}_{\xi_{\sim i}}\left[Q \mid \xi_i\right]\Big]}{\mathbb{V}ar_{\xi}\left[Q\right]} \qquad \text{and} \qquad \mathbb{T}_i = \frac{\mathbb{E}_{\xi_{\sim i}}\Big[\mathbb{V}ar_{\xi_i}\left[Q \mid \boldsymbol{\xi}_{\sim i}\right]\Big]}{\mathbb{V}ar_{\xi}\left[Q\right]} = 1 - \frac{\mathbb{V}ar_{\xi_{\sim i}}\Big[\mathbb{E}_{\xi_i}\left[Q \mid \boldsymbol{\xi}_{\sim i}\right]\Big]}{\mathbb{V}ar_{\xi}\left[Q\right]}, \tag{2}$$

where $\mathbb{S}_i$ describes the main effect contribution of parameter ξ_i and $\mathbb{T}_i$ describes the effect of parameter ξ_i *and* its interaction with all of the other parameters $\xi_{\sim i}$. By definition, for parameter ξ_i, $0 \leq \mathbb{S}_i \leq \mathbb{T}_i$, where the difference $\mathbb{T}_i - \mathbb{S}_i$ captures the effect solely of ξ_i's interactions. Additionally by definition, $\sum_{i=1}^{k} \mathbb{S}_i \leq 1$, where the difference $1 - \sum_{i=1}^{k} \mathbb{S}_i$ provides an idea of how much variance remains to be captured by higher-order effects; refer to [4] for additional details.

The so-called Saltelli method [4] is a sampling-based approach to estimate the full suite of first- and total-order SIs. We outline the general algorithm of this approach below, assuming k uncertain parameters:

1. Define two (N_ξ, k) matrices, $\boldsymbol{A}$ and $\boldsymbol{B}$, which contain independent input samples.

$$\boldsymbol{A} = \begin{bmatrix} \xi_1^{(1)} & \cdots & \xi_i^{(1)} & \cdots & \xi_k^{(1)} \\ \vdots & & \ddots & & \vdots \\ \xi_1^{(N)} & \cdots & \xi_i^{(N_\xi)} & \cdots & \xi_k^{(N_\xi)} \end{bmatrix}, \qquad \boldsymbol{B} = \begin{bmatrix} \xi_{k+1}^{(1)} & \cdots & \xi_{k+i}^{(1)} & \cdots & \xi_{2k}^{(1)} \\ \vdots & & \ddots & & \vdots \\ \xi_{k+1}^{(N_\xi)} & \cdots & \xi_{k+i}^{(N_\xi)} & \cdots & \xi_{2k}^{(N_\xi)} \end{bmatrix}.$$

2. For each i-th input factor, define matrix $\boldsymbol{A}_{\boldsymbol{B}}^{(\boldsymbol{i})}$, which is a copy of $\boldsymbol{A}$ except for the i-th column, which comes from $\boldsymbol{B}$.

$$\boldsymbol{A}_{\boldsymbol{B}}^{(\boldsymbol{i})} = \begin{bmatrix} \xi_1^{(1)} & \cdots & \xi_{k+i}^{(1)} & \cdots & \xi_k^{(1)} \\ \vdots & & \ddots & & \vdots \\ \xi_1^{(N_\xi)} & \cdots & \xi_{k+i}^{(N_\xi)} & \cdots & \xi_k^{(N_\xi)} \end{bmatrix}.$$

3. Compute model output for $\boldsymbol{A}$, $\boldsymbol{B}$, and all $\boldsymbol{A}_{\boldsymbol{B}}^{(\boldsymbol{i})}$ to obtain vectors of model output $Q(\boldsymbol{A})$, $Q(\boldsymbol{B})$, and $Q(\boldsymbol{A}_{\boldsymbol{B}}^{(\boldsymbol{i})})$, all of dimension $(N_\xi, 1)$. Let $Q(\boldsymbol{A})_v$ indicate the v-th element of the vector $Q(\boldsymbol{A})$, i.e., one function evaluation of Q.
4. Approximate the full set of $\mathbb{S}_i$ and $\mathbb{T}_i$ using $Q(\boldsymbol{A})$, $Q(\boldsymbol{B})$ and $Q(\boldsymbol{A}_{\boldsymbol{B}}^{(\boldsymbol{i})})$:

$$\mathbb{S}_i \approx \frac{\frac{1}{N_\xi}\sum_{v=1}^{N_\xi} Q(\boldsymbol{B})_v \left[Q(\boldsymbol{A}_{\boldsymbol{B}}^{(\boldsymbol{i})})_v - Q(\boldsymbol{A})_v\right]}{\frac{1}{2N_\xi}\sum_{v=1}^{N_\xi}\Big[Q(\boldsymbol{A})_v - Q(\boldsymbol{B})_v\Big]^2} \stackrel{\text{def}}{=} \hat{\mathbb{S}}_i, \tag{3}$$

$$\mathbb{T}_i \approx \frac{\frac{1}{2N_\xi}\sum_{v=1}^{N_\xi}\Big[Q(\boldsymbol{B}_{\boldsymbol{A}}^{(\boldsymbol{i})})_v - Q(\boldsymbol{B})_v\Big]^2}{\frac{1}{2N_\xi}\sum_{v=1}^{N_\xi}\Big[Q(\boldsymbol{A})_v - Q(\boldsymbol{B})_v\Big]^2} \stackrel{\text{def}}{=} \hat{\mathbb{T}}_i. \tag{4}$$

A number of sampling schemes (e.g., quasi-random sequencing, Latin hypercube) can be used to fulfill step 1) of the above algorithm; for simplicity, we use purely random sampling. To approximate $\mathbb{S}_i$ and $\mathbb{T}_i$ in step 4), we have used a sampling estimator for $\mathbb{S}_i$ from [10] and for $\mathbb{T}_i$ from [11], as recommended for general use by [12]. For a broad review of sampling schemes and estimators used with the Saltelli method, see e.g., [13]. In the following, we describe how to compute the statistical quantities introduced above via sampling when the underlying QoI is computed using a stochastic solver.

2.2. Variance deconvolution

To enable mathematical treatment of the stochastic solver's variability, we represent it with an additional random variable η and define our QoI Q as the expectation over η of a function $f(\boldsymbol{\xi}, \eta)$: $Q(\boldsymbol{\xi}) = \mathbb{E}\left[f(\boldsymbol{\xi}, \eta) \mid \boldsymbol{\xi}\right] \stackrel{\text{def}}{=} \mathbb{E}_\eta\left[f(\boldsymbol{\xi}, \eta)\right]$. The function $f(\boldsymbol{\xi}, \eta)$ can be directly evaluated as the output from the stochastic solver with input $\boldsymbol{\xi}$, but the expectation $\mathbb{E}_\eta\left[f(\boldsymbol{\xi}, \eta)\right]$ and variance $\mathbb{V}ar_\eta\left[f(\boldsymbol{\xi}, \eta)\right] \stackrel{\text{def}}{=} \sigma_\eta^2(\boldsymbol{\xi})$ are not directly available. Instead, we approximate $Q(\boldsymbol{\xi})$ and $\sigma_\eta^2(\xi)$ as the sample mean and variance of f over N_η independent evaluations:

$$Q\left(\boldsymbol{\xi}\right) \approx \frac{1}{N_\eta}\sum_{j=1}^{N_\eta} f(\boldsymbol{\xi}, \eta^{(j)}) \stackrel{\text{def}}{=} \widetilde{Q}_{N_\eta}(\boldsymbol{\xi}) \quad \text{and} \quad \sigma_\eta^2(\boldsymbol{\xi}) \approx \frac{1}{N_\eta - 1}\sum_{j=1}^{N_\eta}\left(f(\boldsymbol{\xi}, \eta^{(j)}) - \widetilde{Q}_{N_\eta}(\boldsymbol{\xi})\right)^2 \stackrel{\text{def}}{=} \hat{\sigma}_\eta^2(\boldsymbol{\xi}).$$

In the context of MC RT, $\eta^{(j)}$ corresponds to the internal stream of random numbers comprising a single particle history, $f(\boldsymbol{\xi}, \eta^{(j)})$ corresponds to the result (e.g., tally) of that single particle history, and $\widetilde{Q}_{N_\eta}(\boldsymbol{\xi})$ corresponds to the output of a MC RT simulation that used a total of N_η particle histories. Variance deconvolution was introduced [5, 6] to show that the parametric variance of Q, $\mathbb{V}ar_\xi\left[Q\right]$, can be efficiently and accurately estimated from $\widetilde{Q}_{N_\eta}$ by explicitly computing and removing the solver variance from the total observed variance. From [5], the total variance of $\widetilde{Q}_{N_\eta}$ decomposes into the effect of the uncertain parameters and the effect of the stochastic solver: $\mathbb{V}ar_\xi\left[Q\right] = \mathbb{V}ar\left[\widetilde{Q}_{N_\eta}\right] - \frac{1}{N_\eta}\mathbb{E}_\xi\left[\sigma_\eta^2\right]$. Building on [5, 7], we have extended variance deconvolution to examine the first- and total-order SIs of ξ_i on $\widetilde{Q}_{N_\eta}$,

$$\mathbb{S}_{i,\widetilde{Q}_{N_\eta}} = \frac{\mathbb{V}ar_{\xi_i}\left[\mathbb{E}_{\xi_{\sim i},\eta}\left[\widetilde{Q}_{N_\eta} \mid \xi_i\right]\right]}{\mathbb{V}ar\left[\widetilde{Q}_{N_\eta}\right]} = \frac{\mathbb{V}ar_{\xi_i}\left[\mathbb{E}_{\xi_{\sim i}}\left[Q \mid \xi_i\right]\right]}{\mathbb{V}ar_\xi\left[Q\right] + \frac{1}{N_\eta}\mathbb{E}_\xi\left[\sigma_\eta^2\right]} \qquad \text{and} \tag{5}$$

$$\mathbb{T}_{i,\widetilde{Q}_{N_\eta}} = \frac{\mathbb{E}_{\xi_{\sim i}}\left[\mathbb{V}ar_{\xi,\eta}\left[\widetilde{Q}_{N_\eta} \mid \xi_{\sim i}\right]\right]}{\mathbb{V}ar\left[\widetilde{Q}_{N_\eta}\right]} = \frac{\mathbb{E}_{\xi_{\sim i}}\left[\mathbb{V}ar_{\xi_i}\left[Q \mid \xi_{\sim i}\right]\right] + \frac{1}{N_\eta}\mathbb{E}_\xi\left[\sigma_\eta^2\right]}{\mathbb{V}ar_\xi\left[Q\right] + \frac{1}{N_\eta}\mathbb{E}_\xi\left[\sigma_\eta^2\right]}. \tag{6}$$

Ongoing theoretical work suggests that $\mathbb{S}_{i,\widetilde{Q}_{N_\eta}}$ will always be less than $\mathbb{S}_i$, therefore *underestimating* the first-order effect of ξ_i on Q, while $\mathbb{T}_{i,\widetilde{Q}_{N_\eta}}$ will always be greater than $\mathbb{T}_i$, therefore *overestimating* the total-order effect of ξ_i on Q. In pursuit of unbiased estimators for $\mathbb{S}_i$ and $\mathbb{T}_i$ using $\widetilde{Q}_{N_\eta}$, we introduce bias-correction terms to the numerator of Eq. (6) and the denominators of both Equations (5) and (6).

Steps 1) and 2) of the GSA algorithm in Section 2.1 remain the same. When evaluating the model for $\boldsymbol{A}$, $\boldsymbol{B}$, and all $\boldsymbol{A}_{\boldsymbol{B}}^{(\boldsymbol{i})}$ in Step 3), variance deconvolution requires tallying the variance $\hat{\sigma}_\eta^2(\boldsymbol{\xi})$ in addition to the model output $\widetilde{Q}_{N_\eta}(\boldsymbol{\xi})$. In practice, every independent code evaluation for $\widetilde{Q}_{N_\eta}(\boldsymbol{\xi})$ should also be independent in η, that is, each MC RT code evaluation should use a different initial random number seed. Then, in Step 4),

Equations (3) and (4) are replaced with

$$\mathbb{S}_i \approx \hat{\mathbb{S}}_{i,VD} \overset{\text{def}}{=} \frac{\frac{1}{N_\xi}\sum_{v=1}^{N_\xi} \widetilde{Q}_{N_\eta}(\boldsymbol{B})_v \left[\widetilde{Q}_{N_\eta}(\boldsymbol{A}_{\boldsymbol{B}}^{(i)})_v - \widetilde{Q}_{N_\eta}(\boldsymbol{A})_v\right]}{\frac{1}{2N_\xi}\sum_{v=1}^{N_\xi}\left[\widetilde{Q}_{N_\eta}(\boldsymbol{A})_v - \widetilde{Q}_{N_\eta}(\boldsymbol{B})_v\right]^2 - \frac{1}{N_\eta}\left\langle\hat{\sigma}_\eta^2\right\rangle_{(A,B)}}, \tag{7}$$

$$\mathbb{T}_i \approx \hat{\mathbb{T}}_{i,VD} \overset{\text{def}}{=} \frac{\frac{1}{2N_\xi}\sum_{v=1}^{N_\xi}\left[\widetilde{Q}_{N_\eta}(\boldsymbol{B}_{\boldsymbol{A}}^{(i)})_v - \widetilde{Q}_{N_\eta}(\boldsymbol{B})_v\right]^2 - \frac{1}{N_\eta}\left\langle\hat{\sigma}_\eta^2\right\rangle_{(B_A^i,B)}}{\frac{1}{2N_\xi}\sum_{v=1}^{N_\xi}\left[\widetilde{Q}_{N_\eta}(\boldsymbol{A})_v - \widetilde{Q}_{N_\eta}(\boldsymbol{B})_v\right]^2 - \frac{1}{N_\eta}\left\langle\hat{\sigma}_\eta^2\right\rangle_{(A,B)}}, \tag{8}$$

where $\left\langle\hat{\sigma}_\eta^2\right\rangle_{(A,B)} = \dfrac{1}{2N_\xi}\displaystyle\sum_{v=1}^{N_\xi}\left[\hat{\sigma}_\eta^2(\boldsymbol{A})_v + \hat{\sigma}_\eta^2(\boldsymbol{B})_v\right]$.

3. NUMERICAL RESULTS

In this section, we first provide a description of the multigroup 3D C5G7 benchmark, on which the k-eigenvalue simulations are based. Then, we present and discuss results of the uncertainty and sensitivity analysis for eight uncertain input parameters: the densities and radii of the four types of fuel in the benchmark.

3.1. 3D C5G7 Benchmark Description

The C5G7-TD benchmark is a series of space-time neutron kinetics exercises in 2- and 3D [8] based on the well-studied 2-D steady-state neutron transport C5G7 benchmark [14]. We performed a k-eigenvalue simulation of the initial condition of 3D geometry described by the C5G7-TD benchmark, i.e., the unrodded case in which the control rod banks are inserted into the upper axial water reflector.

3D C5G7 is a miniature LWR with sixteen fuel assemblies: eight uranium oxide (UO_2) assemblies and eight mixed oxide (MOX) assemblies, surrounded by a water reflector. There are three different enrichments of MOX fuel: 4.3%, 7.0%, and 8.7%. The quarter-core is radially symmetric in the 2-D plane, and it is assumed that control rods can move continuously across the top water reflector into the active core region. Both the UO2 and MOX assemblies follow a 17 x 17 configuration, consisting of 264 fuel pins, 24 guide tubes for control rods, and one instrument tube for a fission chamber in the center grid cell. The quarter-core with assemblies labeled 1-4 and the fuel-pin configuration are shown in Figure 1.

The C5G7 benchmark problems were originally developed to test the capabilities of radiation transport codes that do not utilize spatial homogenization above the fuel pin level. Therefore, the available 7-group macroscopic cross-section data from the original benchmark [14] as well as the kinetics parameters from [8] are spatially homogenized to the fuel pin level. Using all nominal parameter values, the eigenvalue of the unrodded configuration of the 3D C5G7 core was calculated to be $k_{\text{eff}} = 1.16562 \pm 0.02\%$ using MC/DC with a total of 50×10^6 particle histories. Other MC codes [15] found $k_{\text{eff}} = 1.165449 \pm 0.0029\%$ (RMC, 2021) and $k_{\text{eff}} = 1.16532 \pm 0.0034\%$ (OpenMC, 2018).

First, for uncertainty analysis, we consider the parametric variance of k_{eff} and of the pin-wise fission distribution. Then, for sensitivity analysis, we rank the eight parameters in order of importance to k_{eff}.

3.2. Uncertainty analysis

We choose manufacturing uncertainties to follow manufacturing uncertainties of the assembly models described in the OECD/NEA UAM benchmark [16]. For each of the four fuel types in C5G7, the density and diameter of the fuel pin are each normally distributed with a standard deviation of 5%.

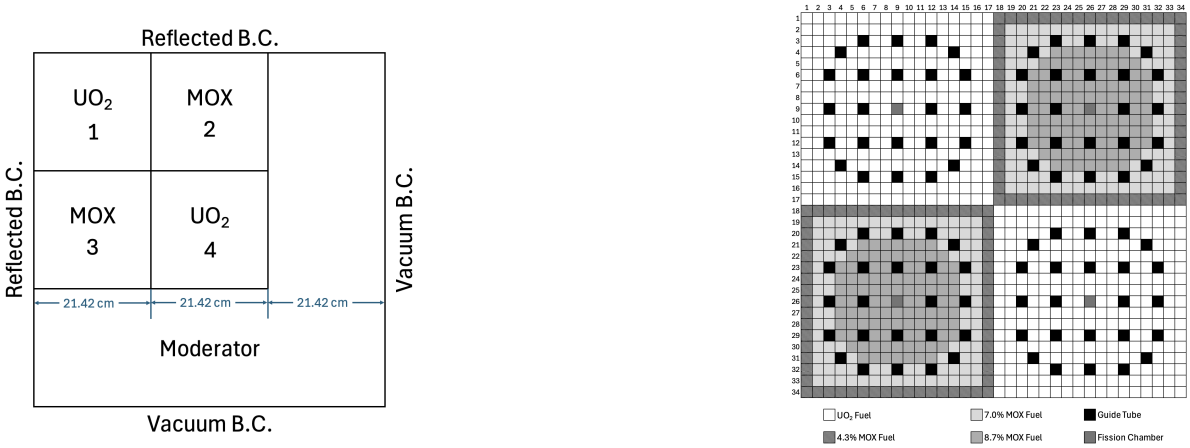

(a) Quarter-core planar section.

(b) Fuel pin configuration.

Figure 1. Geometry of the 3D C5G7 benchmark problem, south-east quadrant, reproduced from [8].

To study the efficiency of variance deconvolution for a k-eigenvalue simulation, we compare the parametric variance estimate from the variance deconvolution approach with the total observed variance estimate from a standard UQ approach, in which the solver variance is assumed to have been effectively resolved out. First, to establish the problem's solver variance with nominal values, we compute k_{eff} and its standard error σ_k using 50 inactive cycles, 100 active cycles, and 50K histories per cycle for a total of 5M histories. This case is labeled 'Ref.' in Table I, with the total observed standard error of k_{eff} resulting entirely from the solver stochasticity. Then, in Case A, we minimize the solver noise by repeating the reference case 100 times for a total of 500M histories, reducing $\sigma_{k,\text{MCRT}}/k_{\text{eff}}$ from 0.054% to 0.007%. Next, for the standard UQ approach in Case B, we vary all 8 parameters and perform the simulation 100 times with 50 inactive cycles, 100 active cycles, and 50K histories/cycle for a total of 500M histories. Comparing Cases A and

Case	Description	k_{eff}	$\sigma_{k,\text{total}}$	$\sigma_{k,\text{param}}$	$\sigma_{k,\text{MCRT}}$
Ref.	Nominal parameter values. 5M total histories.	1.16568	0.00064	N/A	0.00064
A	Nominal parameter values. 500M total histories.	1.16562	0.00008	N/A	0.00008
B	Standard UQ. $N_\xi = 100$, 500M total histories.	1.15817	**0.00209**	N/A	N/A
C	Variance deconvolution. $N_\xi = 100$, 10M total histories.	1.15799	0.00214	**0.00208**	0.00048

Table I. Resulting k_{eff} from varying parameters in 3D C5G7 problem. $\sigma_{k,\text{total}}$, $\sigma_{k,\text{param}}$, and $\sigma_{k,\text{MCRT}}$ represent the 1-sigma standard deviation of k_{eff} due to the overall simulation uncertainty, the parameter uncertainty, and the MC RT solver noise, respectively.

B, we see that $\sigma_{k,\text{total}}$ in Case A is small compared to that of Case B and we can conclude that almost all the uncertainty in Case B is due to the uncertain parameters. To confirm this, we continue to increase the resolution of the MC RT simulation to observe that $\sigma_{k,\text{total}}$ does not diminish any further. Next, for the variance deconvolution approach in Case C, we reduce to 1K histories/cycle for a total of 10M histories, a 50X reduction in computational cost from Case B. Comparing Cases B and C, we see that variance deconvolution and standard UQ estimate a $\sigma_{k,\text{param}}$ within 0.5% of one another; variance deconvolution

does so using 50X fewer histories/cycle, which is directly proportional to a reduction in execution time. In Case C with 10M histories, the standard UQ approach would estimate the parametric σ_k as $\sigma_{k,\text{total}}$, 0.00214.

As an additional QoI, we consider the fission rate distribution calculated in Cases B and C. In Figure 2, we compare the variances estimated using the standard approach (Fig. 2a) and the variance deconvolution approach (Figs. 2b- 3b). As in the variance estimates for k_{eff}, the total variance with a standard UQ approach and the parametric variance with the variance deconvolution approach are in agreement. We see that the parametric variance is peaked in the top left corner of Assembly 1, i.e., at the center of the full-core where it is most active. Using a standard UQ approach with 10M histories, the total variance in Figure 3b would be the best available variance estimate. Although the total variance is also the largest in Assembly 1, we can see that it is much less resolved than the sharper relative peaks in Figure 2. Comparing Figures 3a and 3b, we can see the influence that the shape of the solver variance influences the shape of the total variance, and increasing the particle count in Case B provides a clearer image of the impact of the uncertain parameters. Using variance deconvolution, we achieve a comparable resolution for 50X fewer particle histories.

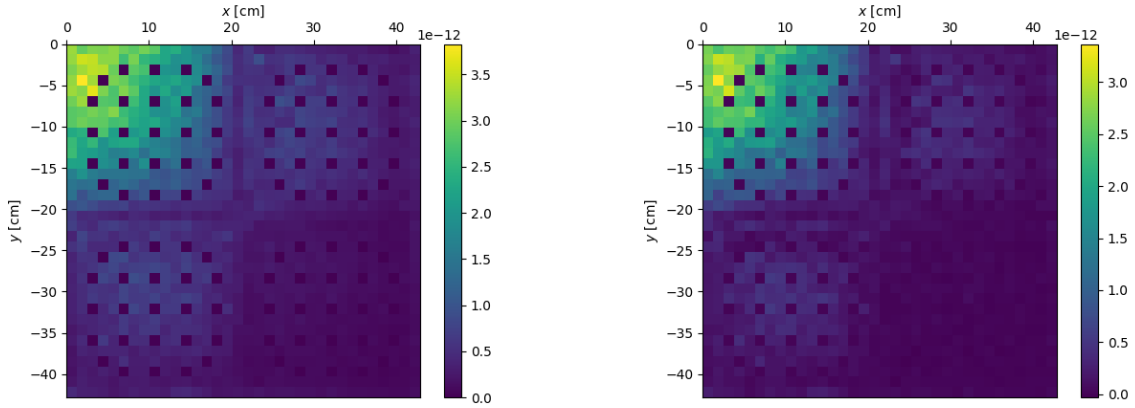

(a) Total variance estimate from Case B, standard UQ, 500M histories.

(b) Parametric variance estimate from Case C, variance deconvolution, 10M histories.

Figure 2. Variance estimates using the standard approach (a) and variance deconvolution approach (b). Fuel pin density and diameter each sampled from normal distribution with 5% standard deviation.

3.3. Sensitivity analysis

Additionally, we compute the first- and total-order sensitivity indices of the 8 parameters with respect to k_{eff}, comparing the standard and variance deconvolution approaches using Case C. We report all computed indices and rank the parameters in Table II. As seen in the data in Table II, $1 - \sum_{i=1}^{k} \mathbb{S}_i = 0.004$, suggesting that the parametric variance is almost entirely comprised of first-order effects. However, $\mathbb{T}_i - \mathbb{S}_i$ ranges between 0.011 and 0.053, suggesting a larger interaction effect than is indicated by the first-order effects alone. We hypothesize that this discrepancy could be due to correlation effects between k_{eff} cycles in a single simulation and that an effective N_η may need to be used rather than taking N_η to be the number of active cycles $\times$ the number of particle histories per cycle. For example, if the solver variance reported by the code were slightly underestimated, it would align with what ongoing theory work suggests that $\mathbb{S}_i$ from variance deconvolution would still be a slight underestimate and $\mathbb{T}_i$ from variance deconvolution would still be a slight overestimate, therefore creating a larger difference between $\mathbb{T}_i$ and $\mathbb{S}_i$. Working through details of this in an orderly way is a topic of ongoing and future work.

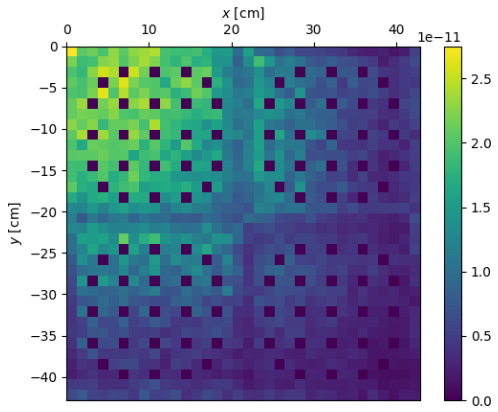

(a) Solver variance estimate from Case C, variance deconvolution, 10M histories.

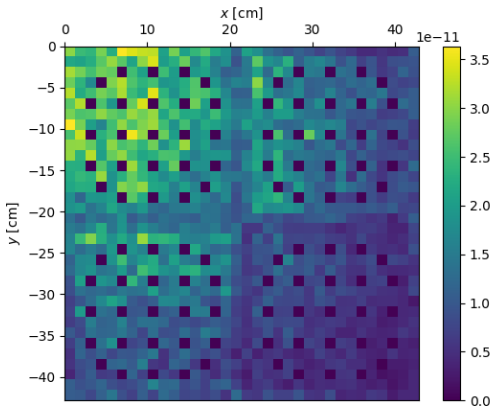

(b) Total variance estimate from Case C, variance deconvolution, 10M histories.

Figure 3. Solver (a) and total (b) variance estimates using the variance deconvolution approach. Fuel pin density and diameter each sampled from normal distribution with 5% standard deviation.

In general, we can conclude that the pin radii have a greater impact than the pin densities, which is consistent with the findings of parameter studies that also varied both the fuel radius and the density [3]. Criticality conditions are very sensitive to geometry changes that would necessarily result from changing the radii of the fuel pin. Additionally, unlike the densities, the radii affect the amount of moderator in the problem: the larger the fuel pins, the less space is available around them for the moderator. The radius of the UO_2 pin is the most important by far; we look to the remaining parameters to highlight the importance of computing the full set of first- *and* total-order indices. One could reasonably set an importance threshold below which parameters are discarded as unimportant, e.g., 0.05 or 0.10. Looking just at the first-order indices, this would qualify most, if not all, of the remaining parameters as unimportant. However, the total-order indices reveal the additional importance contribution of interaction effects. For example, the MOX8. 7% radius nearly doubles from $\mathbb{S}_i = 0.0524$ to $\mathbb{T}_i = 0.1028$. In the same vein, comparing the parametric indices $\mathbb{S}_i$ and $\mathbb{T}_i$ to their total-observed counterparts $\mathbb{S}_{i,\widetilde{\mathcal{Q}}_{N_\eta}}$ and $\mathbb{T}_{i,\widetilde{\mathcal{Q}}_{N_\eta}}$, we see that the standard approach could result in misleading conclusions about the importance of a parameter. Although both approaches rank the parameters in the same order, the standard approach *underestimates* $\mathbb{S}_i$ and *overestimates* $\mathbb{T}_i$. For example, all four densities appear more important from $\mathbb{T}_{i,\widetilde{\mathcal{Q}}_{N_\eta}}$ than they are revealed to be from $\mathbb{T}_i$. This is consistent with the findings discussed in Section 2.2.

4. CONCLUSIONS

Sampling methods for UQ and GSA are useful because they do not make assumptions about the underlying model; their primary drawback is the potentially-high computational cost of the multiple code evaluations they require. When sampling methods are coupled with stochastic simulators such as Monte Carlo radiation transport codes, a standard approach to estimate parametric statistics (i.e., statistics due only to parameter uncertainty) is to increase the number of particle histories such that the solver variance is a relatively small part of the total observed variance, exacerbating sampling methods' primary drawback. As an alternative to attempting to minimize solver variance, we have recently proposed variance deconvolution, in which parametric variance is computed by explicitly quantifying and removing the solver variance from the total observed variance. In previous work, we showed that variance deconvolution is accurate and far more

Parameter	$\mathbb{S}_i$	$\mathbb{T}_i$	$\mathbb{S}_{i,\widetilde{Q}_{N_\eta}}$	$\mathbb{T}_{i,\widetilde{Q}_{N_\eta}}$
1. UO_2 radius	0.7936	0.8043	0.7497	0.8151
2. MOX7.0% radius	0.0680	0.1178	0.0642	0.1666
3. MOX8.7% radius	0.0524	0.1028	0.0495	0.1524
4. MOX4.5% radius	0.0334	0.0851	0.0316	0.1357
5. UO_2 density	0.0176	0.0699	0.0166	0.1213
6. MOX4.5% density	0.0119	0.0647	0.0112	0.1164
7. MOX7.0% density	0.0106	0.0633	0.0100	0.1151
8. MOX8.7% density	0.0085	0.0614	0.0080	0.1133
Sum over all parameters	0.9960	1.3693	0.9409	1.7359

Table II. First- and total-order sensitivity indices of k_{eff} given fuel pin density and diameter each sampled from normal distribution with 5% standard deviation. UO_2 radius is most important to k_{eff} both on its own and with interaction effects.

cost-effective than the standard approach for computing parametric variance [5] and integrated variance deconvolution into sampling estimators for sensitivity indices [7].

In this study, variance deconvolution was coupled with Monte Carlo radiation transport to perform uncertainty quantification and global sensitivity analysis on the 3D C5G7-TD benchmark in its initial unrodded configuration. The C5G7 core was modeled using Monte Carlo Dynamic Code (MC/DC), a neutral-particle transport code from the PSAAP-III Center for Exascale Monte Carlo Neutron Transport [9]. The manufacturing uncertainties of the radius and density of the fuel pin were sampled from a normal distribution with 5% standard deviation, based on the manufacturing uncertainties from the OECD / NEA benchmarks for Uncertainty Analysis in Modeling of LWRs. The core k_{eff} eigenvalue and pinwise core fission rate distribution were considered as quantities of interest. Using 50 inactive cycles, 100 active cycles, and 100 samples of the uncertain parameters, $\sigma_{k,\text{param}}/k_{\text{eff}}$ was estimated to be 0.18% using the standard approach with 50K histories per cycle and using the variance deconvolution approach with 1K histories per cycle, a 50X reduction in computational cost. Though the exact savings in computation time will vary from code-to-code, reducing particle count consistently reduces code execution time. Both the standard approach and variance deconvolution approach found the fuel-pin radii to be more important than their densities, consistent with findings from similar studies. Indices computed with the standard approach were observed to underestimate first-order and overestimate total-order indices, which is in alignment with what ongoing theory work suggests. Ongoing and future work include presenting the details and theoretical explanation of this behavior and investigating use of effective particle numbers in sensitivity coefficient calculations. Future work also includes extending these methods to correlated input parameters, as existing variance deconvolution analysis has been based on the assumption that parameters are independently distributed. This extension would allow for application to jointly-distributed parameters such as nuclear data uncertainty, which is highly relevant to the field.

ACKNOWLEDGEMENTS

This article has been authored by an employee of National Technology & Engineering Solutions of Sandia, LLC under Contract No. DE-NA0003525 with the U.S. Department of Energy (DOE). The employee owns all right, title and interest in and to the article and is solely responsible for its contents. The United States Government retains and the publisher, by accepting the article for publication, acknowledges that the United States Government retains a non-exclusive, paid-up, irrevocable, world-wide license to publish or reproduce the published form of this article or allow others to do so, for United States Government purposes. The

DOE will provide public access to these results of federally sponsored research in accordance with the DOE Public Access Plan https://www.energy.gov/downloads/doe-public-access-plan. This work was funded by the Center for Exascale Monte Carlo Neutron Transport (CEMeNT) a PSAAP-III project funded by the Department of Energy, grant number: DE-NA003967.

REFERENCES

[1] M. Jessee and D. Dehart. "Generalized Perturbation Theory Capability within the SCALE Code Package." In *Proceedings of M&C 2009*. American Nuclear Society (2009).

[2] D. Rochman et al. "Efficient Use of Monte Carlo: Uncertainty Propagation." *Nuclear Science and Engineering*, **volume 177** (2014).

[3] F. Brown, J. Sweezy, and R. Hayes. "Monte Carlo Parameter Studies and Uncertainty Analysis with MCNP5." In *Proceedings of PHYSOR 2004*. PHYSOR, Chicago, Illinois, USA (2004).

[4] A. Saltelli et al. *Global Sensitivity Analysis: The Primer*. John Wiley & Sons, United Kingdom (2008).

[5] K. Clements et al. "A Variance Deconvolution Estimator for Efficient Uncertainty Quantification in Monte Carlo Radiation Transport Applications." *Jrnl of Quant Spect and Rad Trans* (2024).

[6] A. J. Olson. "Calculation of parametric variance using variance deconvolution." In *Transactions of the American Nuclear Society*, volume 120 (2019).

[7] K. Clements et al. "Global sensitivity analysis in Monte Carlo radiation transport." In *Proceedings of M&C 2023*. American Nuclear Society (2023).

[8] J. Hou et al. "OECD/NEA benchmark for time-dependent neutron transport calculations without spatial homogenization." *Nuclear Engineering and Design*, **volume 317**, pp. 177–189 (2017).

[9] J. P. Morgan et al. "Monte Carlo / Dynamic Code (MC/DC): An accelerated Python package for fully transient neutron transport and rapid methods development." *Journal of Open Source Software*, **volume 9**, p. 6415 (2024). URL https://joss.theoj.org/papers/10.21105/joss.06415.

[10] I. Sobol' et al. "Estimating the approximation error when fixing unessential factors in global sensitivity analysis." *Reliability Engineering and System Safety*, **volume 97**(7), pp. 957–960 (2007).

[11] M. Jansen. "Analysis of Variance Designs for Model Output." *Computer Physics Communications*, **volume 117**(1-2), pp. 35–43 (1999).

[12] A. Saltelli, M. Ratto, S. Tarantola, and F. Campolongo. "Update 1 of: sensitivity analysis for chemical models." *Journal of Chemistry*, **volume 112**(5), pp. PR1–PR21 (2012).

[13] A. Puy, S. L. Piano, A. Saltelli, and S. Levin. "Sensobol: An R package to compute variance-based sensitivity indices." *Journal of Statistical Software*, **volume 102** (2022).

[14] N. S. Committee. "Benchmark on deterministic transport calculations without spatial homogenization." Technical report, OECD/NEA (2005).

[15] X. Guo et al. "Kinetic methods in Monte Carlo code RMC and its implementation to C5G7-TD benchmark." *Annals of Nuclear Energy* (2021).

[16] K. Ivanov et al. "Benchmarks for Uncertainty Analysis in Modeling (UAM) for the Design, Operation and Safety Analysis of LWRs." Technical Report NEA/NSC/DOC(2013)7, OECD/NEA (2013).